THE JOURNAL OF PHYSICAL CHEMISTRY A
A JOURNAL OF THE AMERICAN CHEMICAL SOCIETY

pubs.acs.org/JPCA Article

Acidity-Dependent Atmospheric Organosulfate Structures and Spectra: Exploration of Protonation State Effects via Raman and Infrared Spectroscopies Combined with Density Functional Theory

Published as part of The Journal of Physical Chemistry virtual special issue "Advances in Atmospheric Chemical and Physical Processes".

Alison M. Fankhauser, Ziying Lei, Kimberly R. Daley, Yao Xiao, Zhenfa Zhang, Avram Gold, Bruce S. Ault, Jason D. Surratt, and Andrew P. Ault*

Cite This: J. Phys. Chem. A 2022, 126, 5974−5984 Read Online

ACCESS | Metrics & More | Article Recommendations | Supporting Information

ABSTRACT: Organosulfates formed from heterogeneous reactions of organic-derived oxidation products with sulfate ions can account for >15% of secondary organic aerosol (SOA) mass, primarily in submicron particles with long atmospheric lifetimes. However, fundamental understanding of organosulfate molecular structures is limited, particularly at atmospherically relevant acidities (pH = 0−6). Herein, for 2-methyltetrol sulfates (2-MTSs), an important group of isoprene-derived organosulfates, protonation state and vibrational modes were studied using Raman and infrared spectroscopy, as well as density functional theory (DFT) calculations of vibrational spectra for neutral ($RO-SO_3H$) and anionic/deprotonated ($RO-SO_3^-$) structures. The calculated sulfate group vibrations differ for the two protonation states due to their different sulfur−oxygen bond orders (1 or 2 versus $1^2/_3$ for the neutral and deprotonated forms, respectively). Only vibrations at 1060 and 1041 cm^{-1}, which are associated with symmetric S−O stretches of the 2-MTS anion, were observed experimentally with Raman, while sulfate group vibrations for the neutral form (~900, 1200, and 1400 cm^{-1}) were not observed. Additional calculations of organosulfates formed from other SOA-precursor gases (α-pinene, β-caryophyllene, and toluene) identified similar symmetric vibrations between 1000 and 1100 cm^{-1} for $RO-SO_3^-$, consistent with corresponding organosulfates formed during laboratory experiments. These results suggest that organosulfates are primarily deprotonated at atmospheric pH values, which have further implications for aerosol acidity, heterogeneous reactions, and continuing chemistry in atmospheric aerosols.

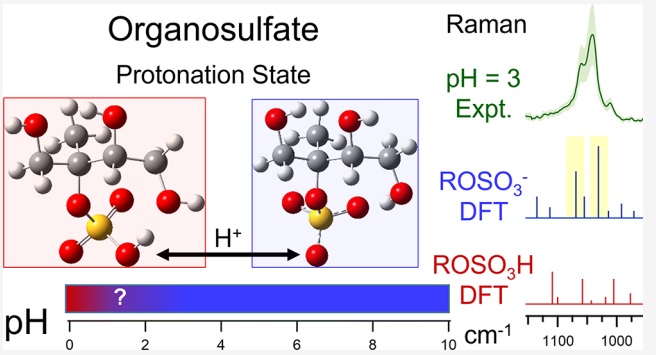

INTRODUCTION

Ambient aerosols have large impacts globally due to their significant climate and health impacts, with exposure to particulate matter (PM) killing 8.9 million people annually.[1] Aerosols also modify climate by scattering or absorbing solar radiation, as well as nucleating cloud droplets and ice crystals, with aerosols currently representing the largest uncertainty with respect to Earth's energy budget.[2−4] Organic aerosol particles are ubiquitous globally,[5] with a large fraction of fine PM ($PM_{2.5}$, mass of particles < 2.5 μm in diameter) coming from secondary organic aerosol (SOA) (20−80%). SOA results from the oxidation of volatile organic compounds (VOCs) to form lower volatility products that are taken up into the condensed (particle) phase.[6] Due to their role in climate change and negative health outcomes, there is a need to better understand formation mechanisms, composition, and properties of SOA.[6−8]

Isoprene has the second highest emissions of any VOC (500−750 Tg yr^{-1}),[9,10] and its two double bonds are primarily oxidized by the hydroxyl radical (OH) during the daytime. As shown by Paulot et al.,[11] OH-driven photochemical reactions of isoprene produce epoxides, such as isoprene epoxydiols (IEPOX) in high yields. Due to its lower vapor pressure (~0.3 Pa)[12] and high Henry's Law Constant (~10^6−10^8 M/atm),[13−17] IEPOX rapidly forms SOA via acid-driven reactive uptake onto ambient aerosols.[11,18] Atmospheric aerosols are primarily acidic, ranging from pH < 0 to 6,[19] with pH ≈ 1−3 the most common for particles less than 2.5 μm.[19,20] Under the acidic conditions

Received: June 29, 2022
Revised: August 16, 2022
Published: August 26, 2022

https://doi.org/10.1021/acs.jpca.2c04548
J. Phys. Chem. A 2022, 126, 5974−5984

common in the atmosphere, the reactive uptake of IEPOX and other epoxides is rapid.[11,18,21−25]

Sulfate (SO_4^{2-}) is another ubiquitous component of atmospheric aerosols formed from the oxidation of sulfur dioxide (SO_2) emitted from anthropogenic and natural sources,[26,27] which represents a large fraction of $PM_{2.5}$ mass.[28] At low pH, protonated epoxides in the presence of sulfate ions form organosulfates via nucleophilic attack leading to a ring-opening reaction, including diastereomeric 2-methyltetrol sulfates (2-MTSs).[29−32] 2-MTSs have been identified at high levels in ambient aerosols from numerous locations[25,29−31,33−35] and were recently shown to comprise ∼13% of the total organic mass in $PM_{2.5}$ collected from Atlanta.[36] The ubiquitous presence and high concentrations of isoprene-derived organosulfates make understanding their molecular properties critical.

Riva et al.[37] recently showed that significant fractions of inorganic sulfate anions (40−90%) are incorporated into organosulfates when IEPOX is exposed to acidic particles, which will alter both the physicochemical properties and composition of aerosols.[38] Current thermodynamic models used to calculate aerosol acidity, such as the Extended Aerosol Inorganics Model (E-AIM)[39,40] and ISORROPIA-II,[41,42] are based on the concentration of inorganic components in addition to temperature and relative humidity. The dynamic relationship between inorganic-to-organic sulfate conversion and protonation state of organosulfates is still poorly understood.

Herein, we investigated the dependence of organosulfate protonation on particle acidity. We report here a detailed analysis of the molecular structure and vibrational modes of 2-MTSs from isoprene oxidation as a case study for the behavior of atmospherically relevant organosulfates. We then explored sulfate vibrational modes for organosulfates formed from other VOCs (α-pinene, β-caryophyllene, and toluene). Synthesized 2-MTSs standards were studied using Raman microspectroscopy, attenuated total reflectance Fourier transform infrared (ATR-FTIR) spectroscopy, atomic force microscopy coupled with photothermal infrared (AFM-PTIR) spectroscopy, and optical photothermal infrared (O-PTIR) spectroscopy. Density functional theory (DFT) was used to identify the lowest energy structures and to connect modes with experimental peak assignments from the experimental Raman and IR spectra; specifically, vibrational modes associated with $RO-SO_3^-$ and $RO-SO_3H$. Organosulfate peaks were systematically explored as a function of pH for the 2-MTSs, and at most pH values, deprotonated organosulfates were abundant. The molecular characterization of isoprene-derived 2-MTSs and organosulfates from other VOCs will aid in future studies of ambient and laboratory-generated organosulfates, which will help in understanding SOA formation under a broad range of atmospheric conditions.

EXPERIMENTAL METHODS

Reagents. A diastereomeric mixture of racemic 2-MTSs (racemic 2-methylerythritol sulfate ester and racemic 2-methylthreitol sulfate ester) was synthesized following the method described in Cui et al.[43] Briefly, 2-methyltetrols were sulfated by pyridine-SO_3, after first protecting the primary and secondary hydroxyl groups by acetylation with acetic anhydride. The acetyl groups were removed by ammonia to yield 2-MTSs as NH_4^+ salts. The resulting 2-MTSs were 85% pure, with a 15% impurity of $(NH_4)_2SO_4$ and a trace impurity of acetamide and were used without further purification. The identity and purity of 2-MTSs were verified by nuclear magnetic resonance (NMR). The pH of the synthesized 2-MTS standard was determined to be 1.3 ± 0.3 using pH indicator paper, according to the procedure outlined by Craig et al.[44]

Sample Preparation. 2-MTSs were dissolved in 18.2 MΩ Milli-Q water to make a 14 mM solution. The pH of the solution of 2-MTSs dissolved in water is 3 as measured by an electronic pH probe (HI2002 edge pH, Hanna Instruments). To explore the effect of pH, H_2SO_4 or NH_4OH was added dropwise into aliquots of 2-MTSs solution to control the bulk solution pH at values varying between 0 and 10. This pH range was chosen because 2-MTSs are hydrolyzed[45,46] under highly acidic conditions (pH < 0) and break down at more basic conditions (pH > 10). Each aliquot was well mixed, and the pH values were measured using the pH probe.

Raman Microspectroscopy. Aqueous 2 μL droplets were pipetted onto quartz substrates (Ted Pella Inc.) and analyzed using a Raman microspectrometer (LabRAM HR Evolution, HORIBA, Ltd.) at laboratory relative humidity (30−40%) and temperature (20−25 °C). The Raman spectrometer was equipped with a confocal optical microscope (100× SLMP long working distance Olympus objective, 0.9 numerical aperture) and a CCD detector. A 532 nm Nd:YAG laser source (32 mW) passed through a neutral density filter at 100% transmission. An 1800 groove/mm diffraction grating was used, yielding ∼0.7 cm^{-1} spectral resolution. Calibrations for the Raman spectrometer were conducted every 24 h using a silicon wafer standard against the Stokes Raman signal of pure Si at 520 cm^{-1}.[47] Sample spectra were collected with three accumulations at 15 s acquisition times from 500 to 4000 cm^{-1}, during which the droplets noticeably evaporated under the laser, but spectra were consistent. The experimental Raman spectra shown in subsequent figures are each an average of five spectra and normalized by the quartz mode at 800 cm^{-1}.

Photothermal Infrared Spectroscopy (PTIR). Atomic force microscopy photothermal infrared spectroscopy (AFM-PTIR; Bruker, Santa Barbara, CA) was used to collect PTIR spectra of the 2-MTS standard on a silicon substrate (Ted Pella Inc.). AFM-PTIR consists of an AFM integrated with a quantum cascade laser (QCL) source with a tuning range of 880 to 1950 cm^{-1} and an average spectral resolution of 2 cm^{-1} and an optical parametric oscillator (OPO) laser that covers the 2700−3600 cm^{-1} window with 4 cm^{-1} spectral resolution. The PTIR spectra were collected in tapping IR mode using a gold coated microfabricated silicon probe (Bruker, Santa Barbara, CA). The tip had a resonance frequency of 70 kHz and spring strength of 1−7 N. IR spectra were collected at a scan rate of 100 cm^{-1} s^{-1}. We note that at the time of collection, that the third and fourth chips of the QCL laser between 1420 and 1700 cm^{-1} were either not functioning correctly, there was an alignment issue, or there was an issue with the AFM tip resulting in limited signal in this region of the spectrum.

To complement the AFM-PTIR results, optical photothermal infrared (O-PTIR) spectroscopy was also used. The mIRage infrared + Raman microscope (Photothermal Spectroscopy Corp.) consists of a visible objective (4×, 0.13 numerical aperture, 17.3 mm working distance, Nikon Plan Fluor), a Cassegrain reflective objective for simultaneous use of IR and visible lasers (40×, 0.78 numerical aperture, 8.3 mm working distance, 55 μm × 42 μm field of view), and the same QCL laser (880 to 1950 cm^{-1}) and OPO laser (2700−3600 cm^{-1}). This instrument was recently developed and used to characterize submicron aerosol particles without contacting the sample,[48] unlike AFM-PTIR. The instrument and theory have been

https://doi.org/10.1021/acs.jpca.2c04548
J. Phys. Chem. A 2022, 126, 5974−5984

described in detail in a previous study.[49] For this application, PTIR spectra were collected at a scan rate of 100 cm^{-1}/s for 15 s acquisitions and averaged over three accumulations. The IR laser repetition rate was set at 100 kHz and 300 ns per pulse, and the IR power and visible laser were set to approximately 4−10 mW each. An average of 10 spectra were collected for each 2-MTS sample.

Attenuated Total Reflectance-Fourier Transform Infrared (ATR-FTIR) Spectroscopy. Bulk 2-MTS standard was transferred to the ATR crystal and analyzed using a Thermo Nicolet iS50 FTIR spectrometer (Thermo Scientific). An FTIR spectrum was collected from 400 to 4000 cm^{-1} at a resolution of 4 cm^{-1} and averaged over 32 scans at ambient temperature (~25 °C).

Density Functional Theory Calculations. Theoretical calculations were carried out on the organosulfate species considered in this study using the Gaussian 16 and 16W suite of programs.[50] DFT calculations used the hybrid B3LYP functional to locate energy minima, determine structures, and calculate vibrational spectra. Final calculations with full geometry optimization employed the 6-311++G(3df,3pd) basis set, after initial calculations with lower-level basis sets were run to approximate the energy minima. This level of theory has previously been shown to effectively reproduce organosulfate vibrational frequencies.[25] All calculated frequencies presented in this manuscript are unscaled.

RESULTS AND DISCUSSION

Given the range of aerosol acidities in the atmosphere (~0−6)[19] and unknown pK_a of 2-methyltetrol sulfate esters (2-MTSs),[38] it is important to understand both the neutral and deprotonated structures. Since the synthetic standard is a racemic mixture of 2-MTSs diastereomers (2-methylerythritol sulfate ester and 2-methylthreitol sulfate ester), molecular structures were calculated for both. 2-MTS skeletal structural formulas without stereochemistry are shown in Figure 1A,C for the anionic (2-MTS$^-$) and neutral forms (2-MTSH), respectively. Optimized structures from DFT are shown for both protonation states of 2-methylerythritol sulfate ester in Figure 1B,D. Corresponding optimized structures for the anionic and neutral forms of 2-methylthreitol sulfate ester are shown in Figure S1 in the Supporting Information. Given a lack of appreciable differences in the calculated structures and spectra (see below), 2-methylerythritol sulfate ester is discussed henceforth in the manuscript and referred to as 2-MTS.

To provide greater confidence that the calculated structure above was the lowest energy structure, energies of multiple rotamers of the different enantiomers of the deprotonated and neutral 2-MTS were calculated. Different internal rotations in these species can lead to a range of structures, particularly for molecules such as the 2-MTSs with multiple functional groups capable of hydrogen bonding and the potential for differing numbers of internal hydrogen bonds. For the 2-MTS$^-$ anion, three sample rotamers were calculated, one with no internal hydrogen bonding, one with a single hydrogen bond, and one with two hydrogen bonds. As expected, the rotamer with two internal hydrogen bonds (one hydroxyl to sulfate moiety and the two other hydroxyl groups hydrogen bonding with each other) has the lowest energy, followed by a rotamer with two hydrogen bonds to the sulfate moiety that is 1.8 kcal/mol higher in energy, and a rotamer with one hydrogen bond that is 3.2 kcal/mol higher in energy. The highest in energy was the non-hydrogen bonded rotamer, over 12 kcal/mol higher than the lowest energy

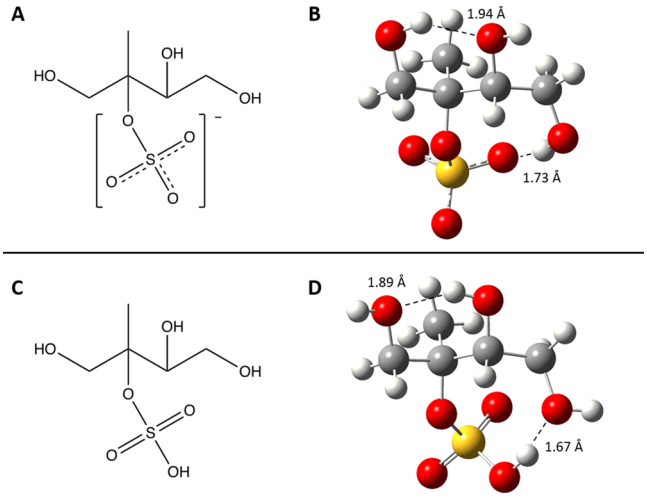

Figure 1. (A) Skeletal formula of the 2-MTS anion (2-MTS$^-$) without stereochemistry. (B) Ball-and-stick model of deprotonated 2-methylerythritol sulfate ester, with hydrogen bonding indicated by dashed lines. (C) Skeletal formula of neutral 2-MTS (2-MTSH) without stereochemistry. (D) Ball-and-stick model of neutral 2-methylerythritol sulfate ester, with hydrogen bonding indicated by dashed lines. Geometry for both ball-and-stick models was optimized with B3LYP/6-311++G(3df,3pd), and spheres were scaled by 75% of their atomic radii. See Supporting Information for skeletal formulas and ball-and-stick models of the anion and neutral of the other diastereomer.

rotamer. It is noteworthy that the calculated vibrational spectra of the three rotamers had quite similar frequencies and intensities, particularly for the vibrations of the sulfate moiety. It is unlikely that there are additional prominent rotamers with vibrational spectra that differ significantly from these three. This provides greater confidence in analyses comparing both experimental and calculated vibrational spectra, as well as between protonation states.

Important distinctions between the anion and neutral structures are evident from the bond order of the sulfur−oxygen bonds of the sulfate groups, as well as the orientation of the sulfate and hydroxyl groups. The 2-MTS$^-$ anion has three equivalent sulfur−oxygen bonds of order $1^2/_3$ due to resonance, whereas the neutral molecule has two equivalent double bonds (S═O) as well as a single bond (S−O) between sulfur and the protonated oxygen. The order of the other S−O bond where the sulfate group bonds to the carbon backbone is the same between the structures of the two protonation states.

Both 2-MTS protonation states show the sulfate group hydrogen bonding to the hydroxyl group on the C4 terminal carbon. However, depending on the protonation state, the sulfate and hydroxyl groups rotate, and the hydrogen bonding switches from the oxygen of the sulfate group and the hydrogen of the C4 hydroxyl group for 2-MTS$^-$ (1.73 Å) to the hydrogen of the sulfate group and the oxygen of the C4 hydroxyl group for 2-MTSH (1.67 Å), resulting in a slightly shorter H-bond, indicative of a stronger H-bond, for the neutral structure. Additionally, while not interacting with the sulfate groups, the remaining two hydroxyl groups of each structure interact with each other. For the 2-MTS anion, the hydrogen of the C1 terminal hydroxyl group hydrogen bonds to the oxygen of the C3 hydroxyl group (1.94 Å). For the neutral 2-MTSH, the oxygen of the C1 terminal hydroxyl group hydrogen bonds to the hydrogen of the C3 hydroxyl group (1.89 Å). The

https://doi.org/10.1021/acs.jpca.2c04548
J. Phys. Chem. A 2022, 126, 5974−5984

orientation of these hydrogen-bonded hydroxyl groups for the anionic and neutral forms shifts approximately 180° at the same time the C4 terminal hydroxyl rotates based on the protonation state of the sulfate group. As is evident from the H-bond lengths, hydrogen bonding of the hydroxyl groups is not as strong as the hydrogen bonding involving the sulfate functional groups. The structural differences observed between the different molecules illustrated in Figure 1 result in distinct differences in the Raman and IR spectra, as discussed below.

It is important to identify the key modes in the 2-MTS Raman spectra and correlate them with spectra calculated from the optimized structures in Figure 1, as 2-MTSs are much more abundant than 3-methyltetrol sulfates (3-MTS),[36,37,51] which are the other isoprene-derived organosulfates to be analyzed with both Raman and DFT (though not previously with IR).[25] Figure 2 shows an experimental Raman spectrum of the synthetic 2-MTS standard dissolved in water at pH = 3 (green), as well as the calculated Raman spectra of the anion (blue) and neutral (red) forms of 2-MTS. Calculated vibrational spectra (Raman and IR) for the other diastereomer of 2-MTS are shown in Figures S2–S5. The vibrational spectra and the accompanying animations of vibrational motion provided by Gaussian are used to determine peak assignments, and DFT modes corresponding to sulfur−oxygen stretches are emphasized with thicker and darker lines pointed to by a vertical arrow. Due to the similarity in frequency and relative intensity of two major peaks between the experimental and calculated anion spectra (1041 and 1060 cm^{-1} versus 1031 and 1069 cm^{-1}, respectively), as well as the absence of the major peak (1209 cm^{-1}) in the calculated neutral spectra, 2-MTS likely exists primarily in its deprotonated form at pH = 3.

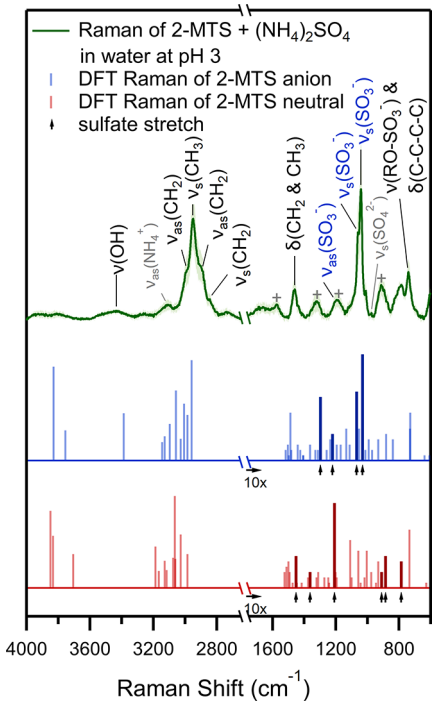

Figure 2. Experimental Raman spectrum of aqueous 2-MTS droplets initially at pH = 3 (green) and calculated Raman spectra of anion (blue) and neutral (red) forms of 2-MTS. The experimental Raman data shown is an average of five measurements with the light green shading showing their standard deviation, which is small indicating the reproducibility of the spectra. Thicker and darker lines emphasized by vertical arrows indicate DFT modes associated with stretching of a sulfur−oxygen bond. Due to similarities with the DFT anion spectrum, 2-MTS is likely to be deprotonated in the experimental spectrum, and consistent assignments are labeled. Labels written in gray denote assignments for inorganic residual species from 2-MTS synthesis. Note that the intensity scale of the lower frequency modes in the DFT spectra (511−1750 cm^{-1}) is enhanced 10× in comparison to the higher frequency modes (2650−3600 cm^{-1}) to improve legibility. Cross (+) denotes fluorescence.

The strong modes at 1041 and 1060 cm^{-1} are assigned to the symmetric stretch of the sulfate group, $\nu_s(SO_3^-)$, which is consistent with a bond order ($1^2/_3$) roughly halfway between that of a S−O single bond (900 cm^{-1}) and a S═O double bond (1200 cm^{-1}).[52] While one SO_3^- symmetric stretch is anticipated for the isolated anion based on group theoretical analysis,[52] two bands are observed here in this region. This is due to strong coupling of the SO_3^- symmetric stretch to a stretching mode of the carbon skeleton of the organic substituent in this spectral region. This coupling leads to "borrowing or sharing of intensity" and the presence of two bands of comparable intensity. On the other hand, the symmetric stretch of the HSO_3 unit in the neutral molecule comes around 900 cm^{-1}, not near the stretching mode of the carbon skeleton. As a result, coupling does not occur. These observations are borne out clearly when the DFT-calculated vibrations are animated. It should be noted that bisulfate has a vibration ∼1040 cm^{-1} as well,[53−56] but not at ∼1060 cm^{-1}, making 1060 cm^{-1} the more unambiguous marker for $\nu_s(SO_3^-)$ from organosulfates.

The mode at 741 cm^{-1} is attributed to overlapping peaks from a skeletal mode of the carbon backbone, δ(C−C−C−C), and stretching of the S−O bond where the sulfate group bonds to the carbon backbone, ν(RO−SO_3^-). The mode at 1202 cm^{-1} is assigned to the sulfate group antisymmetric stretch, $\nu_{as}(SO_3^-)$, which has much weaker Raman scattering than the $\nu_s(SO_3^-)$ mode. The peak at 1460 cm^{-1} corresponds to bending of the methylene and methyl groups, δ(CH_2 and CH_3), while stretches (ν(CH_2) and ν(CH_3)) are observed between 2800 and 3100 cm^{-1}. Greater deviations between experimental and calculated spectra were observed for the C−H stretching modes due to the anharmonic nature of the potential surface. Higher frequency vibrations sample a higher energy portion of the potential well, a portion which is more anharmonic than the lower energy region.[57] In contrast, Gaussian applies the harmonic oscillator approximation to calculate vibrational frequencies, leading to greater differences between experiment and calculation for higher frequency modes. The weak, broad mode between 3350 and 3600 cm^{-1} is assigned to both stretching of the hydroxyl groups, ν(OH), and contributions from water, with the broad nature due to hydrogen bonding. Residual aqueous sulfate and ammonium impurities from synthesis are present at 976 and 3113 cm^{-1}, consistent with $\nu_s(SO_4^{2-})$[58−60] and $\nu_{as}(NH_4^+)$,[61] respectively. Table 1 summarizes the vibrational assignments for the experimental and calculated Raman active peaks of 2-MTS^-. All frequencies and intensities from the DFT calculations, are given in Tables S1 and S2, for 2-MTS^- and 2-MTSH, respectively. Tentative vibrational assignments for observed modes not assigned to the organosulfate molecule, such as those from inorganic residuals from synthesis and fluorescent byproducts (discussed in more detail below), are given in Table S3.

According to the work of Darer et al.[45] and Hu et al.,[46] isoprene-derived tertiary organosulfates are less thermodynamically stable than isoprene-derived organosulfates with primary

https://doi.org/10.1021/acs.jpca.2c04548
J. Phys. Chem. A 2022, 126, 5974−5984

Table 1. Peak Assignments for Experimental and Calculated Raman Spectra of 2-MTS Anion. Frequencies Units Are cm^{-1}

Raman Frequencies (cm^{-1})		
Experimental	Calculated (Anion)	Assignment
741	730	δ(C−C−C−C)
	731	ν(RO−SO_3^-)
1041	1031	ν_s(SO_3^-)
1060	1069	ν_s(SO_3^-)
1202	1221	ν_{as}(SO_3^-)
1460	1487	δ(CH_2 and CH_3)
2846	2959	ν_s(CH_2)
2894	3007	ν_{as}(CH_2)
2953	3059	ν_s(CH_3)
2988	3097	ν_{as}(CH_2)
∼3350−3600	3831	ν(OH)

and secondary sulfate groups, which leads the tertiary organosulfates to undergo hydrolysis much more quickly under strong acidic conditions (pH < 0). Nevertheless, 2-MTSs are predicted to be stable against hydrolysis at pH > 0 on the time scale of atmospheric particle lifetimes (1−2 days). Due to this stability, pH effects on vibrational spectra were explored.

Figure 3 depicts aqueous phase experimental Raman spectra of 2-MTS at pH = 0.05, 0.58, 0.96, 1.53, 1.95, 2.07, 2.41, 2.95,

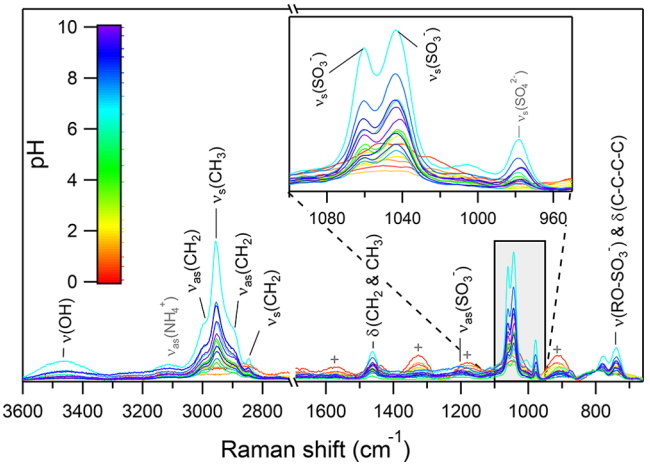

Figure 3. Raman spectra of 2-MTS in aqueous droplets (experimental) normalized by quartz substrate mode. Acidity of droplet indicated by color bar. Assignments are consistent with the deprotonated 2-MTS shown in Figure 2. Below pH = 2, certain modes, including those identified with a cross (+), are likely the result of fluorescent reaction products.

3.93, 4.57, 5.22, 5.89, 6.60, 7.31, 7.84, 8.23, 8.86, 9.18, 9.70, and 10.03. In general, the spectra for pH values above 2 are very similar to the spectrum at pH 3 shown in Figure 2. While these spectra vary in intensity across acidities, there was no apparent trend as a function of pH. Below pH = 2, new peaks denoted with a cross are clearly evident at 915, 1181, 1326, and 1575 cm^{-1}, while the definition of the ν_s(SO_3^-) modes decreases significantly. Due to the simultaneous decay of modes associated with C−H stretching between 2800 and 3100 cm^{-1} as well as visible browning of our initially colorless droplets under the more acidic conditions (see Figure S6), we hypothesize that these peaks are the results of fluorescent degradation products formed by photochemistry involving photons from the 532 nm laser, potentially due to dehydration, and are a focus of future work.

Figure 4 depicts the experimental ATR-FTIR spectrum of 2-MTS (green) and the calculated IR spectra for deprotonated

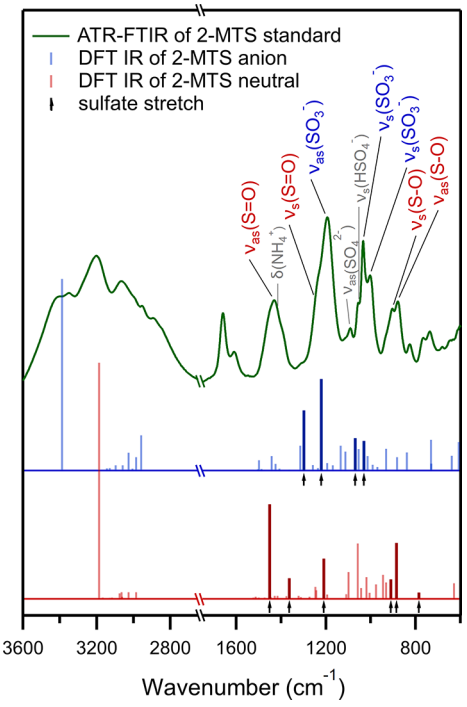

Figure 4. Experimental ATR-FTIR spectrum of 2-MTS standard (green) and calculated DFT IR spectra of anion (blue) and neutral (red) forms of 2-MTS. Thicker and darker lines emphasized by vertical arrows indicate DFT modes associated with stretching of a sulfur−oxygen bond. 2-MTS is assumed to be a mixture of anion and neutral forms in the experimental spectrum, and consistent assignments are labeled with corresponding colors. Labels written in gray denote assignments for inorganic residual species from 2-MTS synthesis.

(blue) and protonated (red) 2-MTS from DFT. Notably the pure standard analyzed had a much lower pH (1.3 ± 0.3) than the aqueous droplet (pH = 3) used in Figure 2. As a result, the experimental IR spectrum suggests the presence of a mixture of anionic and neutral forms of 2-MTSs in the standard. The calculated infrared active modes associated with the sulfur−oxygen stretches, emphasized with thicker and darker lines and pointed to by a vertical arrow, are very strong. Peak fitting was used to deconvolute overlapping peaks in the experimental spectrum that appear as a broad peak with a shoulder, such as those around 1200 and 1450 cm^{-1}. Modes at 1004 and 1034 cm^{-1} were assigned to ν_s(SO_3^-) and 1196 cm^{-1} to ν_{as}(SO_3^-) from the 2-MTS anion. Peaks at 886 and 911 cm^{-1} are attributed to the antisymmetric and symmetric stretches of the neutral 2-MTS sulfur−oxygen single bond, ν(S−O). Peaks at 1209 and 1451 cm^{-1} are attributed to the symmetric and antisymmetric stretches of the neutral 2-MTS sulfur−oxygen double bond, ν(S═O). Note that during ATR-FTIR (and AFM-PTIR) analysis the particles are not exposed to 532 nm light, unlike for Raman and O-PTIR analysis. This may explain the observation of the protonated form rather than degradation products, with photochemistry leading to browning of the sample and fluorescent peaks.

Figure 5 compares the experimental spectra of 2-MTS standard by ATR-FTIR (green), O-PTIR (blue), and AFM-

https://doi.org/10.1021/acs.jpca.2c04548
J. Phys. Chem. A 2022, 126, 5974−5984

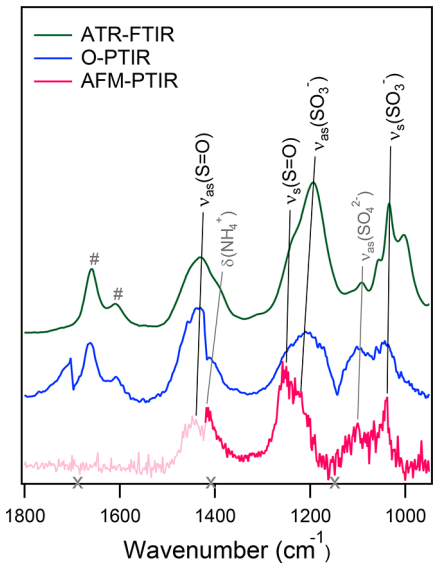

Figure 5. Experimental spectra of pure 2-MTS standard collected by ATR-FTIR (green), O-PTIR (blue), and AFM-PTIR (pink). X marks along the *x*-axis indicate the QCL chip transitions for both PTIR methods. The light pink portion of the AFM-PTIR spectrum indicates a QCL chip performance issue or AFM tip issue and contributes to the uneven chip transition at ∼1420 cm^{-1}. The sharp dip in the O-PTIR spectrum at 1700 cm^{-1} is also related to a chip transition. Hash symbols (#) are for peaks assigned to $\delta(H_2O)$.

PTIR (pink). To our knowledge, these are the first PTIR spectra of 2-MTS. As PTIR is a recently developed approach to allow IR microspectroscopy below the diffraction limit,[48] the generally good agreement between the different techniques supports future use of O-PTIR and AFM-PTIR for probing organosulfates. The $\nu_s(SO_3^-)$ peak assigned to 1034 cm^{-1} for ATR-FTIR is observed at 1035 cm^{-1} for O-PTIR and at 1038 cm^{-1} for AFM-PTIR. Similarly, the peak assigned to $\nu_{as}(SO_3^-)$ at 1196 cm^{-1} for ATR-FTIR, is clearly seen with a maximum at 1221 cm^{-1} by both O-PTIR and AFM-PTIR, whereas the peak assigned to $\nu_s(S{=}O)$ at 1248 cm^{-1} by ATR-FTIR only appears in the AFM-PTIR spectrum at 1258 cm^{-1}. The $\nu_{as}(S{=}O)$ peaks are similar at 1430 cm^{-1} for ATR-FTIR, 1443 cm^{-1} for O-PTIR, and 1448 cm^{-1} for AFM-PTIR. The apparent absence of $\delta(H_2O)$ peaks around 1650 cm^{-1} for AFM-PTIR can be explained by a QCL chip performance issue when the spectrum was collected. The agreement among the spectra affirms confidence in using PTIR to analyze organosulfates in future studies. Table 2 summarizes the tentative vibrational assignments for the experimental and calculated IR active peaks of 2-MTS. Tentative vibrational assignments for observed modes not assigned to the organosulfate, such as those from inorganics, can be found in Table S4.

While experimental microspectroscopy of organosulfate standards provides the most reliable information about the vibrational spectra of these molecules, authentic standards for most atmospherically relevant organosulfates are not available. In the absence of synthesized standards, DFT calculations are extremely valuable. Thus, DFT calculations were performed for several atmospherically relevant organosulfates listed in Table 3 by both their common name and IUPAC name. Therein, the skeletal formula of the compounds and geometry-optimized tube models for both the anion and neutral structures are shown.

The same organosulfates are listed in Table 4 along with their VOC precursors: isoprene, *α*-pinene, *β*-caryophyllene, and

Table 2. Peak Assignments for Experimental IR Spectra of the 2-MTS Standard, as Measured by ATR-FTIR, O-PTIR, and AFM-PTIR, as Well as the Calculated IR Spectra of Anion and Neutral 2-MTS[a]

Experimental IR			Calculated IR			
			Anion		Neutral	
ATR-FTIR	O-PTIR	AFM-PTIR	Freq.	Assign.	Freq.	Assign.
<600	-	-	608	$\delta(SO_3^-)$	541	$\delta(SO_3H)$
737	-	-	731	$\nu(RO{-}SO_3^-)$		
880	-	-			886	$\nu_{as}(S{-}O)$
904	-	-			911	$\nu_s(S{-}O)$
1004	n.d.	n.d.	1031	$\nu_s(SO_3^-)$		
1034	1035	1038	1069	$\nu_s(SO_3^-)$		
1196	1221	1215	1221	$\nu_{as}(SO_3^-)$		
1248	n.d.	1258			1209	$\nu_s(S{=}O)$
1430	1443	1448			1451	$\nu_{as}(S{=}O)$
3065	-	-			3187	$\nu(OH)$
3204	-	-	3388	$\nu(OH)$		

[a]Frequencies have units of cm^{-1}. Dashes (−) indicate out of acquisition range, and n.d. indicates not detected.

toluene. SOA from each of these precursors was generated in a series of laboratory chamber experiments described in Lei et al.,[62] and the major Raman mode associated with the organosulfate products for each are also given. Experimental Raman measurements of the sulfur−oxygen stretches of the available synthetic organosulfate standards, measured in this work and previously by Bondy et al.,[25] are given for the isoprene-derived organosulfates. These modes are associated with the symmetric sulfate stretch of the organosulfate anion. Furthermore, they are consistent with the modes of both the OS-containing isoprene SOA mixture experimentally measured at 1052 cm^{-1}, as well as the DFT calculations for the deprotonated forms of these isoprene-derived OS compounds. While the organosulfates formed from the other three precursors do not have synthesized standards, and consequently do not have experimentally measured Raman modes in Table 4, their experimental SOA measurements also align well with the symmetric stretch of the $1^2/_3$ sulfur−oxygen bonds from the anion DFT calculations. In contrast, the calculated stretches of the single and double sulfur−oxygen bonds of the neutral forms of all organosulfates are 100 cm^{-1} or more away from the measured SOA mixtures.

The vibrational frequencies associated with sulfur−oxygen stretches, as calculated by DFT, are shown in Figure 6. These modes generally do not overlap for the two protonation states for either the Raman- or IR- active modes. Since the organosulfate-containing SOA at atmospherically relevant pH aligns well with the anion calculations, it is expected that organosulfates are primarily deprotonated in ambient aerosols.

CONCLUSION

While organosulfates are ubiquitous globally within atmospheric $PM_{2.5}$, their vibrational modes and their pH-dependent behavior are not well understood. Vibrational analysis of 2-MTSs was carried out across a range of acidities (pH = 0−10) using Raman and infrared spectroscopies (ATR-FTIR, AFM-PTIR, and O-PTIR), and corroborated with DFT calculations using the B3LYP functional with the 6-311++G(3df,3pd) basis set. DFT calculations revealed that the deprotonated spectrum for 2-

https://doi.org/10.1021/acs.jpca.2c04548
J. Phys. Chem. A 2022, 126, 5974−5984

Table 3. Chemical Structures of Atmospherically-Relevant Organosulfates Depicted as Skeletal Formulae and Tube Models[a]

Name	IUPAC Name	Skeletal Formula	Anion Geometry	Neutral Geometry
2-Methyltetrol sulfate (isoprene)	(1,3,4-trihydroxy-2-methylbutan-2-yl) hydrogen sulfate	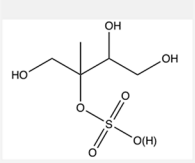		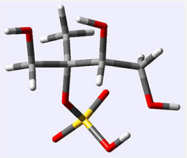
3-Methyltetrol sulfate (isoprene)	(2,3,4-trihydroxy-3-methylbutyl) hydrogen sulfate	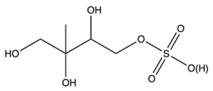	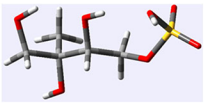	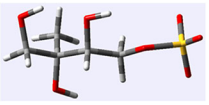
2-Methylglyceric acid sulfate (isoprene)	2-hydroxyl-2-methyl-3-sulfooxypropanoic acid	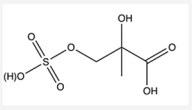		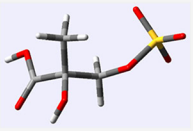
α-Pinene sulfate	(2-hydroxy-2,6,6-trimethyl-3-bicyclo[3.1.1]heptanyl) hydrogen sulfate	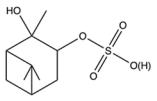	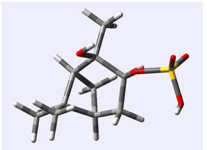	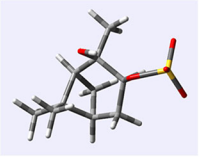
β-Caryophyllene sulfate	(E)-2-hydroxyl-6,10,10-trimethylbicyclo[7.2.0]undec-5-en-2-yl hydrogen sulfate	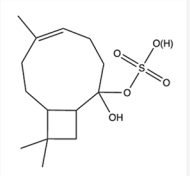	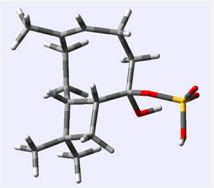	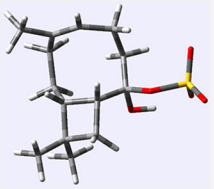
m-Cresol sulfate (toluene)	(3-methylphenyl) hydrogen sulfate	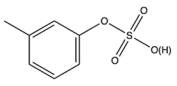	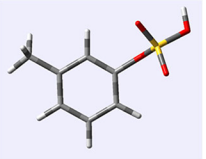	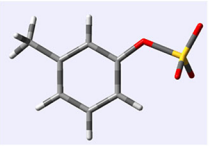

[a]Where not included in name, precursor VOC added in parentheses. Geometry for the tube models were optimized with B3LYP/6-311++G(3df,3pd). 3-Methyltetrol sulfate structures are calculated at a higher level of theory than in Bondy et al.

Table 4. Atmospherically-Relevant Organosulfates, Their Precursors, Sulfur−Oxygen Stretches of Related OS-Containing SOA or Synthesized Standards as Measured Experimentally by Raman Microspectroscopy, and Sulfur−Oxygen Stretches as Calculated by DFT and Distinguished within Parentheses. Asterisk (*) Indicates Experimental Results from This Work

			Anion		Neutral	
		OS-containing SOA mixtures[62]	$\nu_s(SO_3)$		ν(S−O)	ν(S═O)
Molecule	Precursor VOC	Exp	Exp	Calc	Calc	Calc
2-Methyltetrol sulfate*	Isoprene	1052	1041, 1060	(1031, 1069)	(886, 911)	(1209, 1451)
3-Methyltetrol sulfate[25]			1047, 1064	(1029, 1055)	(822, 971)	(1214, 1453)
2-Methylglyceric acid sulfate[25]			1053, 1066	(1031, 1092)	(783, 869)	(1212, 1445)
α-Pinene sulfate	α-Pinene	1072	–	(1004, 1022)	(879, 975)	(1211, 1444)
β-Caryophyllene sulfate	β-Caryophyllene	1072	–	(1042, 1073)	(825, 845)	(1195, 1399)
3-Methylphenyl sulfate	Toluene	1064	–	(1002, 1047)	(862, 944)	(1214, 1434)

https://doi.org/10.1021/acs.jpca.2c04548
J. Phys. Chem. A 2022, 126, 5974−5984

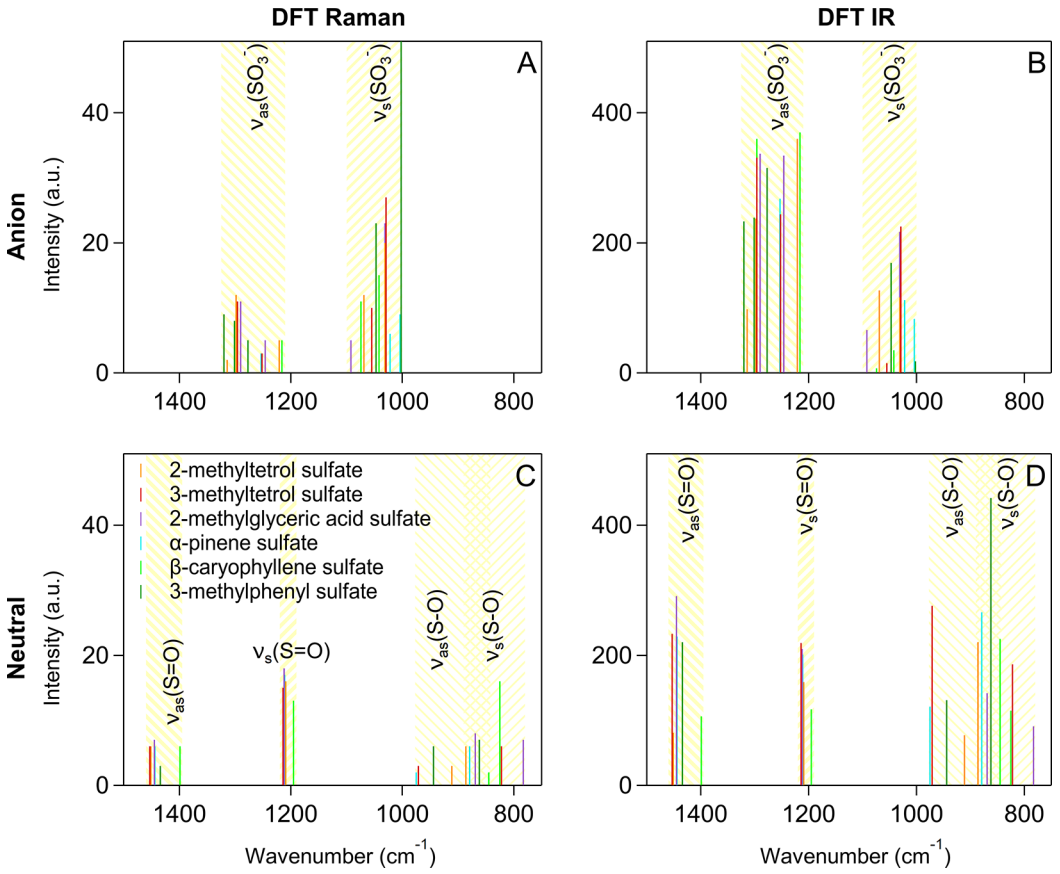

Figure 6. Sulfur−oxygen stretches for atmospherically relevant organosulfates as calculated by DFT. 2-Methyltetrol sulfates, 3-methyltetrol sulfates, and 2-methylglyceric acid sulfates are all derived from isoprene, while 3-methylphenyl sulfates are derived from toluene. For both the IR and Raman calculations, the sulfur−oxygen stretches do not overlap between the anion and neutral structures of the organosulfates.

MTSs was most similar to the experimental Raman and infrared spectra collected.

Distinct organosulfate modes were identified for 2-MTSs and explored for organosulfates formed from other VOC precursors. For the aqueous Raman spectra of 2-MTSs, the strongest modes at 1041 and 1060 cm^{-1} were assigned to $\nu_s(SO_3^-)$. For the infrared spectra of the 2-MTS standard, the modes around 1034 and 1196 cm^{-1} were assigned to $\nu_s(SO_3^-)$ and $\nu_{as}(SO_3^-)$, respectively. Similar sulfur−oxygen stretches were observed in modes for other deprotonated organosulfates calculated for isoprene (i.e., 3-methyltetrol sulfates and 3-methylglyceric acid sulfates), as well as those derived from α-pinene, β-caryophyllene, and toluene. These modes were consistent with those identified for organosulfates formed from those VOC precursors during laboratory SOA formation experiments.[62]

These new physical insights into organosulfate structures and vibrations using synthesized 2-MTS and calculations of other organosulfate vibrational modes will aid in future studies identifying organosulfates in submicron aerosol particles during ambient and laboratory studies. Ultimately these insights will improve understanding of organosulfate behavior in aerosol and guide future representations of these species and their reaction mechanisms in atmospheric models.[63]

■ ASSOCIATED CONTENT

Supporting Information

The Supporting Information is available free of charge at https://pubs.acs.org/doi/10.1021/acs.jpca.2c04548.

Optimized structures of deprotonated and neutral 2-methylthreitol sulfate ester; DFT Raman spectra of deprotonated 2-MTS diastereomers; DFT Raman spectra of neutral 2-MTS diastereomers; DFT IR of deprotonated 2-MTS diastereomers; DFT IR spectra of neutral 2-MTS diastereomers; DFT vibrational frequencies for deprotonated 2-methylerythritol sulfate ester; DFT vibrational frequencies for neutral 2-methylerythritol sulfate ester; Experimental Raman modes not assigned to 2-MTS; Experimental IR modes not assigned to 2-MTS (PDF)

■ AUTHOR INFORMATION

Corresponding Author

Andrew P. Ault − *Department of Chemistry, University of Michigan, Ann Arbor, Michigan 48109, United States;* orcid.org/0000-0002-7313-8559; Phone: 734-763-2283; Email: aulta@umich.edu

Authors

Alison M. Fankhauser − *Department of Chemistry, University of Michigan, Ann Arbor, Michigan 48109, United States;* orcid.org/0000-0002-8303-8308

Ziying Lei − *Department of Environmental Health Sciences, University of Michigan, Ann Arbor, Michigan 48109, United States;* orcid.org/0000-0003-3071-0698

Kimberly R. Daley − *Department of Chemistry, University of Michigan, Ann Arbor, Michigan 48109, United States;* orcid.org/0000-0002-7818-3113

https://doi.org/10.1021/acs.jpca.2c04548
J. Phys. Chem. A 2022, 126, 5974−5984

Yao Xiao − *Department of Chemistry, University of Michigan, Ann Arbor, Michigan 48109, United States;* orcid.org/0000-0003-3661-2845

Zhenfa Zhang − *Department of Environmental Science and Engineering, University of North Carolina, Chapel Hill, North Carolina 27599, United States*

Avram Gold − *Department of Environmental Science and Engineering, University of North Carolina, Chapel Hill, North Carolina 27599, United States;* orcid.org/0000-0003-1383-6635

Bruce S. Ault − *Department of Chemistry, University of Cincinnati, Cincinnati, Ohio 45221, United States;* orcid.org/0000-0003-3355-1960

Jason D. Surratt − *Department of Environmental Science and Engineering, University of North Carolina, Chapel Hill, North Carolina 27599, United States; Department of Chemistry, University of North Carolina, Chapel Hill, North Carolina 27599, United States;* orcid.org/0000-0002-6833-1450

Complete contact information is available at: https://pubs.acs.org/10.1021/acs.jpca.2c04548

Author Contributions

The manuscript was written primarily by A.M.F. and A.P.A. with contributions and editing from the other authors (Z.L., K.R.D., Y.X., Z.Z., A.G., B.S.A., and J.D.S.). Synthesis and characterization was conducted by Z.Z., A.G., and J.D.S. A.M.F., K.R.D., Z.L., and Y.X. collected the experimental data. B.S.A., A.P.A., A.F.M., and K.R.D. conducted and interpreted the computational chemistry work.

Notes

The authors declare no competing financial interest.

■ ACKNOWLEDGMENTS

This project was supported by the National Science Foundation (NSF) through CAREER Award CHE-1654149 (Ault), as well as AGS-2040610 (Ault) and AGS-2039788 (Surratt). The authors acknowledge the Scanning Probe Microscopy facility in the Department of Chemistry at the University of Michigan for use of the AFM-PTIR. The ATR-FTIR was conducted in the Shared Instrument Facility in the Department of Chemistry at the University of Michigan.

■ REFERENCES

(1) Burnett, R.; Chen, H.; Szyszkowicz, M.; Fann, N.; Hubbell, B.; Pope, C. A.; Apte, J. S.; Brauer, M.; Cohen, A.; Weichenthal, S.; et al. Global Estimates of Mortality Associated With Longterm Exposure to Outdoor Fine Particulate Matter. *Proc. Natl. Acad. Sci. U.S.A.* **2018**, *115*, 9592−9597.

(2) Pöschl, U. Atmospheric aerosols: Composition, transformation, climate and health effects. *Angew. Chem., Int. Ed.* **2005**, *44*, 7520−7540.

(3) Prather, K. A.; Hatch, C. D.; Grassian, V. H. Analysis of Atmospheric Aerosols. *Annu. Rev. Anal. Chem.* **2008**, *390*, 485−514.

(4) IPCC. *Climate Change 2013: The Physical Science Basis. Contribution of Working Group I to the Fifth Assessment Report of the Intergovernmental Panel on Climate Change*; Cambridge University Press: Cambridge, United Kingdom and New York, NY, USA, 2013.

(5) Zhang, Q.; Jimenez, J. L.; Canagaratna, M. R.; Allan, J. D.; Coe, H.; Ulbrich, I.; Alfarra, M. R.; Takami, A.; Middlebrook, A. M.; Sun, Y. L.; et al. Ubiquity and Dominance of Oxygenated Species in Organic Aerosols in Anthropogenically-Influenced Northern Hemisphere Midlatitudes. *Geophys. Res. Lett.* **2007**, *34*, 1−6.

(6) Carlton, A. G.; Wiedinmyer, C.; Kroll, J. H. A Review of Secondary Organic Aerosol (SOA) Formation From Isoprene. *Atmos. Chem. Phys.* **2009**, *42*, 4987−5005.

(7) Riva, M.; Budisulistiorini, S. H.; Zhang, Z.; Gold, A.; Surratt, J. D. Chemical characterization of secondary organic aerosol constituents from isoprene ozonolysis in the presence of acidic aerosol. *Atmos. Environ.* **2016**, *130*, 5−13.

(8) Hallquist, M.; Wenger, J. C.; Baltensperger, U.; Rudich, Y.; Simpson, D.; Claeys, M.; Dommen, J.; Donahue, N. M.; George, C.; Goldstein, A. H.; et al. The Formation, Properties and Impact of Secondary Organic Aerosol: Current and Emerging Issues. *Atmos. Chem. Phys.* **2009**, *9*, 5155−5236.

(9) Guenther, A. B.; Jiang, X.; Heald, C. L.; Sakulyanontvittaya, T.; Duhl, T.; Emmons, L. K.; Wang, X. The Model of Emissions of Gases and Aerosols From Nature Version 2.1 (MEGAN2.1): An Extended and Updated Framework for Modeling Biogenic Emissions. *Geosci. Model Dev.* **2012**, *5*, 1471−1492.

(10) Wennberg, P. O.; Bates, K. H.; Crounse, J. D.; Dodson, L. G.; McVay, R. C.; Mertens, L. A.; Nguyen, T. B.; Praske, E.; Schwantes, R. H.; Smarte, M. D.; et al. Gas-Phase Reactions of Isoprene and Its Major Oxidation Products. *Chem. Rev.* **2018**, *118*, 3337−3390.

(11) Paulot, F.; Crounse, J. D.; Kjaergaard, H. G.; Kurten, A.; St. Clair, J. M.; Seinfeld, J. H.; Wennberg, P. O. Unexpected Epoxide Formation in the Gas-Phase Photooxidation of Isoprene. *Science* **2009**, *325*, 730−733.

(12) Pankow, J. F.; Asher, W. E. SIMPOL.1: A simple group contribution method for predicting vapor pressures and enthalpies of vaporization of multifunctional organic compounds. *Atmos. Chem. Phys.* **2008**, *8*, 2773−2796.

(13) Eddingsaas, N. C.; VanderVelde, D. G.; Wennberg, P. O. Kinetics and Products of the Acid-Catalyzed Ring-Opening of Atmospherically Relevant Butyl Epoxy Alcohols. *J. Phys. Chem. A* **2010**, *114* (31), 8106−8113.

(14) Vasilakos, P.; Hu, Y.; Russell, A.; Nenes, A. Determining the Role of Acidity, Fate and Formation of IEPOX-Derived SOA in CMAQ. *Atmosphere* **2021**, *12* (6), 707.

(15) Pye, H. O. T.; Pinder, R. W.; Piletic, I. R.; Xie, Y.; Capps, S. L.; Lin, Y. H.; Surratt, J. D.; Zhang, Z. F.; Gold, A.; Luecken, D. J.; et al. Epoxide Pathways Improve Model Predictions of Isoprene Markers and Reveal Key Role of Acidity in Aerosol Formation. *Environ. Sci. Technol.* **2013**, *47* (19), 11056−11064.

(16) Nguyen, T. B.; Coggon, M. M.; Bates, K. H.; Zhang, X.; Schwantes, R. H.; Schilling, K. A.; Loza, C. L.; Flagan, R. C.; Wennberg, P. O.; Seinfeld, J. H. Organic aerosol formation from the reactive uptake of isoprene epoxydiols (IEPOX) onto non-acidified inorganic seeds. *Atmos. Chem. Phys.* **2014**, *14* (7), 3497−3510.

(17) Chan, M. N.; Surratt, J. D.; Claeys, M.; Edgerton, E. S.; Tanner, R. L.; Shaw, S. L.; Zheng, M.; Knipping, E. M.; Eddingsaas, N. C.; Wennberg, P. O.; et al. Characterization and Quantification of Isoprene-Derived Epoxydiols in Ambient Aerosol in the Southeastern United States. *Environ. Sci. Technol.* **2010**, *44* (12), 4590−4596.

(18) Surratt, J. D.; Chan, A. W. H.; Eddingsaas, N. C.; Chan, M.; Loza, C. L.; Kwan, A. J.; Hersey, S. P.; Flagan, R. C.; Wennberg, P. O.; Seinfeld, J. H. Reactive Intermediates Revealed in Secondary Organic Aerosol Formation from Isoprene. *Proc. Natl. Acad. Sci. U. S. A.* **2010**, *107*, 6640−6645.

(19) Pye, H. O. T.; Nenes, A.; Alexander, B.; Ault, A. P.; Barth, M. C.; Clegg, S. L.; Collett, J. L., Jr; Fahey, K. M.; Hennigan, C. J.; Herrmann, H.; et al. The acidity of atmospheric particles and clouds. *Atmos. Chem. Phys.* **2020**, *20* (8), 4809−4888.

(20) Zheng, G.; Su, H.; Wang, S.; Andreae, M. O.; Pöschl, U.; Cheng, Y. Multiphase buffer theory explains contrasts in atmospheric aerosol acidity. *Science* **2020**, *369* (6509), 1374−1377.

(21) Gaston, C. J.; Riedel, T. P.; Zhang, Z.; Gold, A.; Surratt, J. D.; Thornton, J. A. Reactive uptake of an isoprene-derived epoxydiol to submicron aerosol particles. *Environ. Sci. Technol.* **2014**, *48*, 11178−11186.

(22) Pye, H. O. T.; Pinder, R. W.; Piletic, I. R.; Xie, Y.; Capps, S. L.; Lin, Y. H.; Surratt, J. D.; Zhang, Z.; Gold, A.; Luecken, D. J.; et al. Epoxide Pathways Improve Model Predictions of Isoprene Markers and Reveal Key Role of Acidity in Aerosol Formation. *Environ. Sci. Technol.* **2013**, *47*, 11056−11064.

(23) Riva, M.; Bell, D. M.; Hansen, A. M. K.; Drozd, G. T.; Zhang, Z.; Gold, A.; Imre, D.; Surratt, J. D.; Glasius, M.; Zelenyuk, A. Effect of Organic Coatings, Humidity and Aerosol Acidity on Multiphase Chemistry of Isoprene Epoxydiols. *Environ. Sci. Technol.* **2016**, *50*, 5580−5588.
(24) Surratt, J. D.; Lewandowski, M.; Offenberg, J. H.; Jaoui, M.; Kleindienst, T. E.; Edney, E. O.; Seinfeld, J. H. Effect of Acidity on Secondary Organic Aerosol Formation From Isoprene. *Environ. Sci. Technol.* **2007**, *41*, 5363−5369.
(25) Bondy, A. L.; Craig, R. L.; Zhang, Z.; Gold, A.; Surratt, J. D.; Ault, A. P. Isoprene-Derived Organosulfates: Vibrational Mode Analysis by Raman Spectroscopy, Acidity-Dependent Spectral Modes, and Observation in Individual Atmospheric Particles. *J. Phys. Chem. A* **2018**, *122* (1), 303−315.
(26) Seinfeld, J. H.; Pandis, S. N. *Atmospheric chemistry and physics: from air pollution to climate change*; John Wiley & Sons, 2016.
(27) Aas, W.; Mortier, A.; Bowersox, V.; Cherian, R.; Faluvegi, G.; Fagerli, H.; Hand, J.; Klimont, Z.; Galy-Lacaux, C.; Lehmann, C. M. B.; et al. Global and regional trends of atmospheric sulfur. *Sci. Rep.* **2019**, *9* (1), 953.
(28) Andreae, M. O.; Rosenfeld, D. Aerosol-cloud-precipitation interactions. Part 1. The nature and sources of cloud-active aerosols. *Earth-Sci. Rev.* **2008**, *89* (1−2), 13−41.
(29) Hatch, L. E.; Creamean, J. M.; Ault, A. P.; Surratt, J. D.; Chan, M. N.; Seinfeld, J. H.; Edgerton, E. S.; Su, Y.; Prather, K. A. Measurements of Isoprene-Derived Organosulfates in Ambient Aerosols by Aerosol Time-of-Flight Mass Spectrometry - Part 1: Single Particle Atmospheric Observations in Atlanta. *Environ. Sci. Technol.* **2011**, *45*, 5105−5111.
(30) Hatch, L. E.; Creamean, J. M.; Ault, A. P.; Surratt, J. D.; Chan, M. N.; Seinfeld, J. H.; Edgerton, E. S.; Su, Y.; Prather, K. A. Measurements of Isoprene-Derived Organosulfates in Ambient Aerosols by Aerosol Time-of-Flight Mass Spectrometry - Part 2: Temporal Variability and Formation Mechanisms. *Environ. Sci. Technol.* **2011**, *45*, 8648−8655.
(31) Surratt, J. D.; Gómez-González, Y.; Chan, A. W. H.; Vermeylen, R.; Shahgholi, M.; Kleindienst, T. E.; Edney, E. O.; Offenberg, J. H.; Lewandowski, M.; Jaoui, M.; et al. Organosulfate Formation in Biogenic Secondary Organic Aerosol. *J. Phys. Chem. A* **2008**, *112*, 8345−8378.
(32) Olson, N. E.; Lei, Z.; Craig, R. L.; Zhang, Y.; Chen, Y.; Lambe, A. T.; Zhang, Z.; Gold, A.; Surratt, J. D.; Ault, A. P. Reactive Uptake of Isoprene Epoxydiols Increases the Viscosity of the Core of Phase-Separated Aerosol Particles. *ACS Earth Space Chem.* **2019**, *3* (8), 1402−1414.
(33) Surratt, J. D.; Chan, M. N.; Claeys, M.; Edgerton, E. S.; Tanner, R. L.; Shaw, S. L.; Zheng, M.; Knipping, E. M.; Eddingsaas, N. C.; Wennberg, P. O.; et al. Characterization and Quantification of Isoprene-Derived Epoxydiols in Ambient Aerosol in the Southeastern United States. *Environ. Sci. Technol.* **2010**, *44*, 4590−4596.
(34) Budisulistiorini, S. H.; Li, X.; Bairai, S. T.; Renfro, J.; Liu, Y.; Liu, Y. J.; McKinney, K. A.; Martin, S. T.; McNeill, V. F.; Pye, H. O. T.; et al. Examining the Effects of Anthropogenic Emissions on Isoprene-Derived Secondary Organic Aerosol Formation During the 2013 Southern Oxidant and Aerosol Study (SOAS) at the Look Rock, Tennessee Ground Site. *Atmos. Chem. Phys.* **2015**, *15*, 8871−8888.
(35) Slade, J. H.; Ault, A. P.; Bui, A. T.; Ditto, J. C.; Lei, Z.; Bondy, A. L.; Olson, N. E.; Cook, R. D.; Desrochers, S. J.; Harvey, R. M. Bouncier Particles at Night: Biogenic Secondary Organic Aerosol Chemistry and Sulfate Drive Diel Variations in the Aerosol Phase in a Mixed Forest. *Environ. Sci. Technol.* **2019**, *53*, 4977.
(36) Hettiyadura, A. P. S.; Al-Naiema, I. M.; Hughes, D. D.; Fang, T.; Stone, E. A. Organosulfates in Atlanta, Georgia: Anthropogenic Influences on Biogenic Secondary Organic Aerosol Formation. *Atmos. Chem. Phys.* **2019**, *19*, 3191−3206.
(37) Riva, M.; Chen, Y.; Zhang, Y.; Lei, Z.; Olson, N. E.; Boyer, H. C.; Narayan, S.; Yee, L. D.; Green, H. S.; Cui, T.; et al. Increasing Isoprene Epoxydiol-to-Inorganic Sulfate Aerosol Ratio Results in Extensive Conversion of Inorganic Sulfate to Organosulfur Forms: Implications for Aerosol Physicochemical Properties. *Environ. Sci. Technol.* **2019**, *53*, 8682−8694.
(38) Zhang, Y.; Chen, Y.; Lei, Z.; Olson, N. E.; Riva, M.; Koss, A. R.; Zhang, Z.; Gold, A.; Jayne, J. T.; Worsnop, D. R.; et al. Joint Impacts of Acidity and Viscosity on the Formation of Secondary Organic Aerosol from Isoprene Epoxydiols (IEPOX) in Phase Separated Particles. *ACS Earth Space Chem.* **2019**, *3*, 2646−2658.
(39) Clegg, S. L.; Brimblecombe, P.; Wexler, A. S. Thermodynamic Model of the System H+ - NH4+ - SO42- - NO3- - H2O at Tropospheric Temperatures. *J. Phys. Chem. A* **1998**, *102*, 2137−2154.
(40) Wexler, A. S. Atmospheric aerosol models for systems including the ions H+, NH4+, Na+, SO42-, NO3-, Cl-, Br-, and H2O. *J. Geophys. Res.* **2002**, *107*, 4207.
(41) Fountoukis, C.; Nenes, A. ISORROPIA II: a computationally efficient thermodynamic equilibrium model for K+-Ca2+-Mg2+-NH(4)(+)-Na+-SO42-NO3-Cl-H2O aerosols. *Atmos. Chem. Phys.* **2007**, *7* (17), 4639−4659.
(42) Nenes, A.; Pandis, S. N.; Pilinis, C. Continued development and testing of a new thermodynamic aerosol module for urban and regional air quality models. *Atmos. Environ.* **1999**, *33* (10), 1553−1560.
(43) Cui, T.; Zeng, Z.; Dos Santos, E. O.; Zhang, Z.; Chen, Y.; Zhang, Y.; Rose, C. A.; Budisulistiorini, S. H.; Collins, L. B.; Bodnar, W. M.; et al. Development of a hydrophilic interaction liquid chromatography (HILIC) method for the chemical characterization of water-soluble isoprene epoxydiol (IEPOX)-derived secondary organic aerosol. *Environ. Sci. Processes Impacts* **2018**, *20*, 1524−1536.
(44) Craig, R. L.; Peterson, P. K.; Nandy, L.; Lei, Z.; Hossain, M. A.; Camarena, S.; Dodson, R. A.; Cook, R. D.; Dutcher, C. S.; Ault, A. P. Direct Determination of Aerosol pH: Size-Resolved Measurements of Submicrometer and Supermicrometer Aqueous Particles. *Anal. Chem.* **2018**, *90* (19), 11232−11239.
(45) Darer, A. I.; Cole-Filipiak, N. C.; O'Connor, A. E.; Elrod, M. J. Formation and Stability of Atmospherically Relevant Isoprene-Derived Organosulfates and Organonitrates. *Environ. Sci. Technol.* **2011**, *45*, 1895−1902.
(46) Hu, K. S.; Darer, A. I.; Elrod, M. J. Thermodynamics and kinetics of the hydrolysis of atmospherically relevant organonitrates and organosulfates. *Atmos. Chem. Phys.* **2011**, *11*, 8307−8320.
(47) Craig, R. L.; Bondy, A. L.; Ault, A. P. Surface Enhanced Raman Spectroscopy Enables Observations of Previously Undetectable Secondary Organic Aerosol Components at the Individual Particle Level. *Anal. Chem.* **2015**, *87* (15), 7510−7514.
(48) Olson, N. E.; Xiao, Y.; Lei, Z.; Ault, A. P. Simultaneous Optical Photothermal Infrared (O-PTIR) and Raman Spectroscopy of Submicrometer Atmospheric Particles. *Anal. Chem.* **2020**, *92*, 9932.
(49) Zhang, D.; Li, C.; Zhang, C.; Slipchenko, M. N.; Eakins, G.; Cheng, J.-X. Depth-resolved mid-infrared photothermal imaging of living cells and organisms with submicrometer spatial resolution. *Sci. Adv.* **2016**, *2* (9), No. e1600521.
(50) Frisch, M. J.; Trucks, G. W.; Schlegel, H. B.; Scuseria, G. E.; Robb, M. A.; Cheeseman, J. R.; Scalmani, G.; Barone, V.; Mennucci, B.; Petersson, G. A.; Nakatsuji, H.; Caricato, M.; Li, X.; Hratchian, H. P.; Izmaylov, A. F.; Bloino, J.; Zheng, G.; Sonnenberg, J. L.; Hada, M.; Ehara, M.; Toyota, K.; Fukuda, R.; Hasegawa, J.; Ishida, M.; Nakajima, T.; Honda, Y.; Kitao, O.; Nakai, H.; Vreven, T.; Montgomery, J. A., Jr.; Peralta, J. E.; Ogliaro, F.; Bearpark, M.; Heyd, J. J.; Brothers, E.; Kudin, K. N.; Staroverov, V. N.; Kobayashi, R.; Normand, J.; Raghavachari, K.; Rendell, A.; Burant, J. C.; Iyengar, S. S.; Tomasi, J.; Cossi, M.; Rega, N.; Millam, J. M.; Klene, M.; Knox, J. E.; Cross, J. B.; Bakken, V.; Adamo, C.; Jaramillo, J.; Gomperts, R.; Stratmann, R. E.; Yazyev, O.; Austin, A. J.; Cammi, R.; Pomelli, C.; Ochterski, J. W.; Martin, R. L.; Morokuma, K.; Zakrzewski, V. G.; Voth, G. A.; Salvador, P.; Dannenberg, J. J.; Dapprich, S.; Daniels, A. D.; Farkas, O.; Foresman, J. B.; Ortiz, J. V.; Cioslowski, J.; Fox, D. J. *Gaussian 09*; Gaussian, Inc.: Wallingford, CT, 2009.
(51) Cui, T.; Green, H. S.; Selleck, P. W.; Zhang, Z.; O'Brien, R. E.; Gold, A.; Keywood, M.; Kroll, J. H.; Surratt, J. D. Chemical Characterization of Isoprene- and Monoterpene-Derived Secondary Organic Aerosol Tracers in Remote Marine Aerosols over a Quarter Century. *ACS Earth Space Chem.* **2019**, *3*, 935−946.

https://doi.org/10.1021/acs.jpca.2c04548
J. Phys. Chem. A 2022, 126, 5974−5984

(52) Nakamoto, K. *Infrared and Raman spectra of inorganic and coordination compounds. Part A, Theory and applications in inorganic chemistry*, 6th ed.; Wiley, 2009.
(53) Yacovitch, T. I.; Wende, T.; Jiang, L.; Heine, N.; Meijer, G.; Neumark, D. M.; Asmis, K. R. Infrared Spectroscopy of Hydrated Bisulfate Anion Clusters: $HSO_4^-(H_2O)_{1-16}$. *J. Phys. Chem. Lett.* **2011**, *2* (17), 2135−2140.
(54) Nash, K. L.; Jessica Sully, K.; Horn, A. B. Infrared spectroscopic studies of the low temperature interconversion of sulfuric acid hydrates. *Phys. Chem. Chem. Phys.* **2000**, *2* (21), 4933−4940.
(55) Irish, D. E.; Chen, H. Raman spectral study of bisulfate-sulfate systems. II. Constitution, equilibriums, and ultrafast proton transfer in sulfuric acid. *J. Phys. Chem.* **1971**, *75*, 2672−2681.
(56) Kruus, P.; Hayes, A. C.; Adams, W. Determination of ratios of sulfate to bisulfate ions in aqueous solutions by Raman spectroscopy. *J. Solution Chem.* **1985**, *14*, 117−128.
(57) Levine, I. N. *Molecular spectroscopy*; Wiley and Sons, 1975; Chapter 4, pp 142−159.
(58) Mabrouk, K. B.; Kauffmann, T. H.; Aroui, H.; Fontana, M. D. Raman study of cation effect on sulfate vibration modes in solid state and in aqueous solutions. *J. Raman Spectrosc.* **2013**, *44*, 1603−1608.
(59) Socrates, G. Sulphur and Selenium Compounds. *Infrared and Raman Characteristic Group Frequencies Contents: Tables and Charts* **2004**, 209−227.
(60) Rudolph, W. Structure and Dissociation of the Hydrogen Sulphate Ion in Aqueous Solution over a Broad Temperature Range: A Raman Study. *Zeitschrift für Physikalische Chemie, Bd.* **1996**, *194*, 73−95.
(61) Craig, R. L.; Bondy, A. L.; Ault, A. P. Computer-controlled Raman microspectroscopy (CC-Raman): A method for the rapid characterization of individual atmospheric aerosol particles. *Aerosol Sci. Technol.* **2017**, *51* (9), 1099−1112.
(62) Lei, Z.; Olson, N. E.; Zhang, Y.; Chen, Y.; Lambe, A. T.; Zhang, J.; White, N. J.; Atkin, J. M.; Banaszak Holl, M. M.; Zhang, Z.; et al. Morphology and Viscosity Changes after Reactive Uptake of Isoprene Epoxydiols in Submicrometer Phase Separated Particles with Secondary Organic Aerosol Formed from Different Volatile Organic Compounds. *ACS Earth Space Chem.* **2022**, *6* (4), 871−882.
(63) Gopalakrishnan, S.; Jungwirth, P.; Tobias, D. J.; Allen, H. C. Air-liquid interfaces of aqueous solutions containing ammonium and sulfate: Spectroscopic and molecular dynamics studies. *J. Phys. Chem. B* **2005**, *109*, 8861−8872.

https://doi.org/10.1021/acs.jpca.2c04548
J. Phys. Chem. A 2022, 126, 5974−5984